

Bayesian Signal Matching for Transfer Learning in ERP-Based Brain Computer Interface

Tianwen Ma

Department of Biostatistics and Bioinformatics, Emory University,
Jane E. Huggins

Department of Physical Medicine and Rehabilitation and
Department of Biomedical Engineering, University of Michigan,
and

Jian Kang*

Department of Biostatistics, University of Michigan

Abstract

An Event-Related Potential (ERP)-based Brain-Computer Interface (BCI) Speller System assists people with disabilities to communicate by decoding electroencephalogram (EEG) signals. A P300-ERP embedded in EEG signals arises in response to a rare, but relevant event (target) among a series of irrelevant events (non-target). Different machine learning methods have constructed binary classifiers to detect target events, known as calibration. The existing calibration strategy uses data from participants themselves with lengthy training time. Participants feel bored and distracted, which causes biased P300 estimation and decreased prediction accuracy. To resolve this issue, we propose a Bayesian signal matching (BSM) framework to calibrate EEG signals from a new participant using data from source participants. BSM specifies the joint distribution of stimulus-specific EEG signals among source participants via a Bayesian hierarchical mixture model. We apply the inference strategy. If source and new participants are similar, they share the same set of model parameters; otherwise, they keep their own sets of model parameters; we predict on the testing data using parameters of the baseline cluster directly. Our hierarchical framework can be generalized to other base classifiers with parametric forms. We demonstrate the advantages of BSM using simulations and focus on the real data analysis among participants with neuro-degenerative diseases.

Keywords: Bayesian Method, Mixture Model, Transfer Learning, P300, Brain-Computer Interface, Calibration-Less Framework.

*To whom correspondence should be addressed: jjankang@umich.edu

1 Introduction

1.1 Background

A Brain-Computer Interface (BCI) is a device that interprets brain activity to assist people with severe neuro-muscular diseases with normal communications. An electroencephalogram (EEG)-based BCI speller system is one of the most popular BCI applications, which enables a person to “type” words without using a physical keyboard by decoding the recorded EEG signals. The EEG brain activity has the advantages of non-invasiveness, low cost, and high temporal resolution (Niedermeyer and da Silva, 2005). The P300 event-related potential BCI design, known as the P300 ERP-BCI design (Donchin et al., 2000), is one of the most widely used BCI frameworks and the focus of this work.

An ERP is an event potential in the EEG signals in response to an external event. The P300 ERP is a particular ERP that occurs in response to a rare, but relevant event (i.e., highlighting a group of characters on the screen) among a group of frequent, but irrelevant ones. The relevant (target) P300 ERP usually has a *positive* deflection in voltage with a latency around 300 ms. Here, the latency refers to the time intervals between the onset of the event and the first response peak. Although P300 ERP is the most useful ERP, other types of ERPs, i.e., N200, exist and help interpret and classify brain activity. During the experiment, participants were asked to wear an EEG cap with multiple electrodes, sit next to a virtual screen, and focus on a specific character to spell, denoted as the “target key.” The study applied the row-and-column paradigm (RCP) developed by (Farwell and Donchin, 1988), which is a 6×6 grid with 36 keys. Each event is either a row stimulus or a column stimulus. The order of rows and columns is random, but it loops through all rows and columns every 12 stimuli, known as a sequence. Participants were asked to mentally count whenever they saw a row or column stimulus containing the target key, and do nothing, otherwise. Thus, each sequence always contained exactly two stimuli that

elicited target P300 ERPs.

The left panel of Figure 1 demonstrates the fundamental mechanism of the P300 ERP-BCI design. The virtual screen presents a sequence of stimuli; Participants respond to the stimuli with EEG signals recorded; The machine truncates the EEG signals in a fixed time response window after each stimulus and generates a EEG feature vector. For raw data with multiple electrodes, the ultimate truncated signal segment is achieved by concatenating multi-channel EEG signals. The machine then makes a *binary* decision whether the participant’s brain elicits a target P300 ERP response. After stimulus-specific binary classifier scores are generated, they are converted into character-level probabilities. Finally, the character with the highest probability is selected and shown on the virtual screen. For offline spelling, the final decision per character is usually made after multiple sequence replications. Many machine learning (ML) methods have successfully constructed such binary classifiers for P300 ERPs, including stepwise linear discriminant analysis (swLDA) (Donchin et al., 2000), (Krusienski et al., 2008), support vector machine (SVM) (Kaper et al., 2004), independent component analysis (ICA) (Xu et al., 2004), linear discriminant analysis (LDA) with xDAWN filter (Rivet et al., 2009), convolutional neural network (CNN) (Cecotti and Graser, 2010), and Riemannian geometry (RG) (Barachant et al., 2011). Recently, Ma et al. (2022) attempted to improve prediction accuracy by identifying spatial-temporal discrepancies between target and non-target P300 responses and explicitly addressed the overlapping ERP issue.

1.2 Challenges and Existing Work

The conventional framework for P300 ERP spelling task requires training and testing, known as calibration and free-typing, as well. Typically, participants were asked to copy a multi-character phrase to build a participant-specific training profile. Due to the low signal-to-noise ratio in EEG, current calibration strategy relies on collecting data from

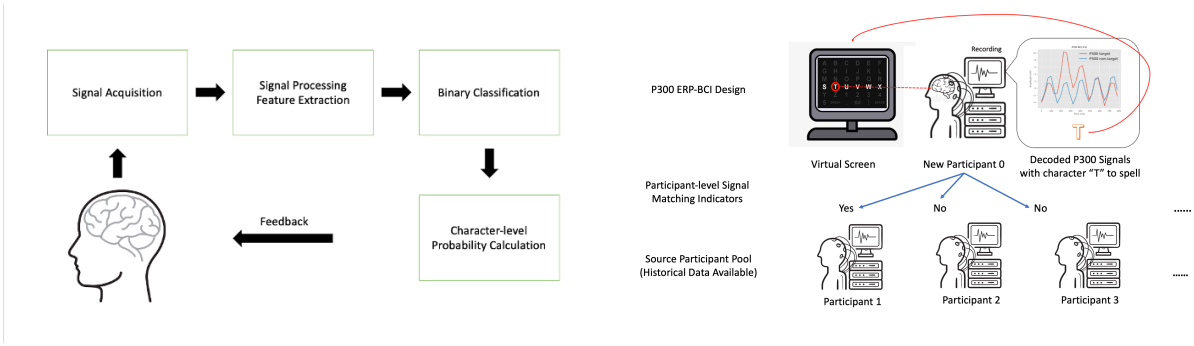


Figure 1: **Left:** The conventional offline framework for P300 ERP spelling includes signal acquisition, pre-processing and feature extraction, binary classification, character-level probability calculation, and final result demonstration. **Right:** The proposed data integration framework leverages data of source participants and small data from the new participant to construct the BSM binary classifier with participant-specific selection indicators.

participants themselves with a fixed but large amount of sequence replications. However, participants tended to feel bored and tired after repetitions, leading to biased target P300 ERPs and inefficient calibration process. Therefore, it is important to identify efficient calibration methods while maintaining decent prediction accuracy for free-typing. Existing work has tackled this problem by applying transfer learning (Bozinovski and Fulgosi, 1976). In statistical fields, we denoted this concept as data integration (Lenzerini, 2002). To avoid confusion, we do not distinguish among “transfer learning,” “data integration,” or “borrowing” in this work. We briefly introduce existing works that have applied transfer learning under different domains with applications to P300 ERP-BCIs. A recent review (Wu et al., 2020) on transfer learning summarized methods between 2016 and 2020 with six paradigms and applications. For P300-ERP BCI paradigm, they considered cross-session/participant and cross-device transfer learning scenarios and produced a nice table for alignment-related approaches including offline/online status, known/unknown labels, alignment framework, referencing objects, base classifiers, and computational costs. We continue introducing the work that were not covered previously.

Ensemble Learning Generic Information (ELGI) (Xu et al., 2015) examined whether inter-participant information is beneficial to ERP classification with simple base classifiers. They applied swLDA to each participant’s dataset as base classifier and combine them to construct the final classifier. Later, they introduced the *Weighted Ensemble Learning Generic Information* (WELGI) (Xu et al., 2016) by adding weights to each base classifier. Similarly, An et al. in 2020 proposed a weighted participant-semi-independent classification method (WSSICM). They applied SVM and fit each base classifier by combining the entire data of each source participant and a small portion of data of the new participant. Weights for base classifiers were determined by an ad-hoc approach. Finally, Adair et al. proposed the *Evolved Ensemble Learning Generic Information* (eELGI) that developed a data-driven algorithm to determine the grouping criterion for training sets among source participants and applied swLDA to form base classifiers.

Transfer learning based on Riemannian geometry (RG) has gained increasing attention recently due to its fast speed to converge and a natural framework to leverage information from source participants. The input data for RG were the sample covariance matrices, and the distance-based algorithm based on RG was called Minimum Distance to Mean (MDM) (Barachant et al., 2011). Congedo et al. and Barachant and Congedo extended the original RG-based classifier to the P300 ERP design by augmenting the covariance matrix with cross-covariance between observed signals and reference target signals. Rodrigues et al. applied the Riemannian procrustes analysis (RPA) to address the heterogeneity of EEG signals across different sessions or participants. Before the authors applied the MDM classifier, they applied certain affine transformations to raw participant-level covariance matrices such that the resulting covariance matrices were less heterogeneous across sessions or participants while their Riemannian distances were preserved. Li et al. standardized the covariance matrices across participants by applying the affine transformation with the participant-specific Riemannian geometric mean covariance matrix. Finally, Khazem et al.

proposed Minimum Distance to Weighted Mean (MDWM) by combining estimated mean covariance matrices from source participants and the new participant via the Riemannian distance with a trade-off hyper-parameter.

1.3 Our Contributions

To reduce the calibration time while maintaining similar prediction accuracy, we proposed a Bayesian Signal Matching (BSM) method to build a participant-dependent, calibration-less framework. BSM reduced the calibration time of a new participant by borrowing data from pre-existing source participants’ pool. We performed an intuitive clustering approach by simply borrowing data from eligible participants without data transformation and homogenization. BSM specified the joint distribution of stimulus-specific EEG signals from all participants via a Bayesian hierarchical mixture model. Our method has several advantages: (i). From the perspective of user experience, fewer training data required for calibration under this framework increased higher spelling efficiency and placed less burden on participants. (ii). From the perspective of inference, we performed pairwise selection between each source participant and the new participant and specified the baseline cluster corresponding to the new participant. The selection indicators represented how close source calibration data of each source participant resembled the data of the new participant. If the selection indicator was 1, we merged source participant’s data with the new participant’s data, otherwise, we kept the source participant’s data as a separate cluster. This approach did not focus on the similarity evaluation among source participants, and thereby, avoided the label-switching issue. (iii). From the perspective of prediction, we used the baseline cluster for *directly* prediction without refitting the model with the augmented data. The applied Bayesian framework for parameter estimation also “leveraged” the shared information from source participants implicitly and was robust to noises. Our proposed hierarchical framework is also flexible to generalize to other classifiers with parametric likelihood func-

tions. (iv). From the perspective of computation, we performed the data analysis on the transformed ERP responses after xDAWN filter (Rivet et al., 2009), The xDAWN filter was a technique for dimensionality reduction. This pre-processing technique increased the signal-to-noise-ratio and matching probability, and improved the modeling efficiency compared to modeling the raw EEG signals or joint modeling transformed EEG signals.

The paper is organized as follows: Sections 2 and 3 present the framework for the Bayesian hierarchical mixture model and posterior inference, respectively. Sections 4 and 5 present the numerical results for simulation and real data analysis, respectively. Section 6 concludes the paper with a discussion.

2 Methods

2.1 Basic Notations and Problem Setup

Let $\mathcal{MVN}(\boldsymbol{\mu}, \Sigma)$ be a multivariate normal distribution with mean and covariance matrix parameters $\boldsymbol{\mu}$ and Σ . Let $\mathcal{MN}(M, U, V)$ be a matrix normal distribution with location matrix M and two scale matrix parameters U and V (Dawid, 1981). Let $\text{Diag}(\cdot)$ be a diagonal matrix notation. Let $\mathcal{LN}(\mu, \sigma)$ be a Log-Normal distribution with mean and scale parameters μ and σ . Let $\mathcal{HC}(x_0, \sigma)$ be a Half-Cauchy distribution with location and scale parameters x_0 and σ . Let $\mathcal{U}(a, b)$ be a Uniform distribution with lower and upper bounds a and b .

Let $n = 0, \dots, N$ be the participant index, where $n = 0$ refers to the new participant and $n = 1, \dots, N$ refer to source participants. Let $l = 1, \dots, L_n$ and $i = 1, \dots, I_n$ be the character index and sequence index for participant n , respectively. We follow the conventional RCP design such that each sequence contains $J(J = 12)$ stimuli, including six row stimuli from top to bottom $(1, \dots, 6)$ and six column stimuli from left to right $(7, \dots, 12)$ on the 6×6 virtual keyboard (See the virtual screen in Figure 1). For the i th

sequence, l th target character, and n th participant, let $\mathbf{W}_{n,l,i} = (W_{n,l,i,1}, \dots, W_{n,l,i,12})^\top$ be a stimulus code indicator that takes values from the permutation of $\{1, \dots, 12\}$. Under the RCP design, given the target character and the stimulus-code indicators, there are exactly two target stimuli and ten non-target stimuli within each sequence. We define $\mathbf{Y}_{n,l,i} = (Y_{n,l,i,1}, \dots, Y_{n,l,i,12})^\top$ as the stimulus-type indicator for the i th sequence, l th target character, and n th participant, where $Y_{n,l,i,j} \in \{0, 1\}$. For example, given a target character “T” and a stimulus code indicator $\mathbf{W}_{n,l,i} = (7, 9, 10, 5, 1, 2, 8, 11, 6, 4, 3, 12)^\top$, we obtain its stimulus type indicator $\mathbf{Y}_{n,l,i} = (0, 0, 0, 0, 0, 0, 1, 0, 0, 1, 0, 0)^\top$, where the indices of 1s correspond to the indices of the 4th row and 2nd column (denoted by 8) in $\mathbf{W}_{n,l,i}$. Let $k = 0, \dots, K - 1$ be the cluster index, where $k = 0$ is the cluster that matches the new participant and $k = 1, \dots, K - 1$ are the clusters within source participants. Finally, we incorporate E channels of EEG signals and let $e (e = 1, \dots, E)$ be the channel index. We extract channel-specific EEG segments from the onset of each stimulus with a long EEG response window length (with T_0 time points). We denote $\mathbf{X}_{n,l,i,j,e}(s)$ as the extracted EEG signal segment of the j th stimulus, i th sequence, l th target character, and n th participant from channel e at time $s \in [0, s_{T_0}]$.

2.2 The Framework of Bayesian Signal Matching

We make three assumptions as follows: (i). We assume that P300 ERPs are the same regardless of target character to spell. To simplify, we let all source participants spell the same character ω with the same sequence replication size I , so we drop the target character index l and the source participant index n from I_n . For example, $Y_{n,l,i,j}$ is reduced to $Y_{n,i,j}$. The biological mechanism behind the speller system is the response to an unexpected stimulus. Under the RCP design, there were always two target stimuli supposed to elicit target P300 ERPs, and this rule applied regardless of the spelling characters. (ii). We assumed that target and non-target ERP functions shared the same covariance matrix

within the same cluster. We simplified the temporal covariance matrix as a scaled AR(1) correlation matrix. Linear discriminant analysis (LDA) with its variations have been shown to be effective binary classifiers for this problem, we argued that the difference on the mean level had sufficient separation effect, and sharing the same covariance matrix reduced the number of parameters. Empirical correlation matrix also suggested that the correlation declined fast and they were similar for target and non-target stimuli, even after the xDAWN filter. The shared and simplified covariance matrix also reduced the number of parameters and made the proposed model parsimonious, especially when we considered borrowing data from source participants. (iii). We performed selection with respect to the target ERP data and we excluded non-target ERP data from the source participants' pool. Despite a larger sample size of non-target ERP data, unfortunately, their signals showed fewer unique patterns and would add more noises to the model fitting. The right panel of Figure 1 provides a detailed illustration of the data integration framework of proposed Bayesian signal matching method. Details of three assumptions can be found in the supplementary material Section S1.

For the new participant, i.e., when $n = 0$, we assume

$$\mathbf{X}_{0,i,j} = \mathbf{B}_{0,1}Y_{0,i,j} + \mathbf{B}_{0,0}(1 - Y_{0,i,j}) + \boldsymbol{\epsilon}_{0,i,j}, \quad (1)$$

where $\mathbf{B}_{0,1}$, $\mathbf{B}_{0,0}$, and $\boldsymbol{\epsilon}_{0,i,j}$ are target ERP matrix, non-target ERP matrix, and random noise matrix of the new participant, of the same size $T_0 \times E$, respectively. For source participant n , $n > 0$, we introduce a participant-specific binary indicator $Z_n \in \{0, 1\}$ and assume that $\Pr(Z_n = 1) = \pi_n$, where π_n is the probability whether source participant n matches the new participant. With $\{Z_n\}$, we consider a signal matching model for the EEG signal matrix for source participant n as follows:

$$\begin{aligned} \mathbf{X}_{n,i,j} &= \mathbf{B}_{n,1}Y_{n,i,j} + \mathbf{B}_{n,0}(1 - Y_{n,i,j}) + \boldsymbol{\epsilon}_{n,i,j}, \\ \mathbf{B}_{n,1} &= \mathbf{B}_{0,1}Z_n + \tilde{\mathbf{B}}_{n,1}(1 - Z_n). \end{aligned} \quad (2)$$

where $\mathbf{B}_{n,1}$, $\tilde{\mathbf{B}}_{n,1}$, $\mathbf{B}_{n,0}$, and $\boldsymbol{\epsilon}_{n,i,j}$ are target ERP matrix after matching, target ERP matrix before matching, non-target ERP matrix, and stimulus-specific random error matrix of source participant n , respectively. Equation (2) assumes that each source participant has either has the new participant's parameter set with a successful matching or their own parameter set. Note that we do not borrow non-target EEG data of source participants. The quantities $\mathbf{X}_{n,i,j}$, $\tilde{\mathbf{B}}_{n,i,j}$, $\mathbf{B}_{n,i,j}$, and $\boldsymbol{\epsilon}_{n,i,j}$ are matrices with the same size of T_0 by E .

For random error matrix $\boldsymbol{\epsilon}_{n,i,j}$, where $n \in \{0, 1, \dots, N\}$, we assume an additive relationship to characterize its spatial-temporal error structure.

$$\begin{aligned}\boldsymbol{\epsilon}_{n,i,j} &= \boldsymbol{\xi}_{n,i,j} + \boldsymbol{\varepsilon}_{n,i,j}, \\ \boldsymbol{\xi}_{n,i,j} &= (\boldsymbol{\xi}_{n,i,j,1}, \dots, \boldsymbol{\xi}_{n,i,j,T_0})^\top, \quad \boldsymbol{\varepsilon}_{n,i,j} = (\boldsymbol{\varepsilon}_{n,i,j,1}, \dots, \boldsymbol{\varepsilon}_{n,i,j,E}),\end{aligned}\tag{3}$$

where $\boldsymbol{\xi}_{n,i,j,t}$, ($t = 1, \dots, T_0$) is a vector of spatial random effects for E channels at time point t , and $\boldsymbol{\varepsilon}_{n,i,j,e}$, ($e = 1, \dots, E$) is a vector of temporal random effects for T_0 time points of channel e . Let $\boldsymbol{\Sigma}_n^s = \mathbf{V}_n \mathbf{R}_n^s \mathbf{V}_n^\top$, \mathbf{R}_n^s , and \mathbf{R}_n^t be the spatial covariance matrix, spatial correlation matrix, and temporal correlation matrix for participant n , $n \in \{0, \dots, N\}$, respectively. \mathbf{R}_n^s is a correlation matrix with the structure of compound symmetry characterized by a scale parameter $\eta_n \in (0, 1)$; \mathbf{V}_k is a diagonal matrix characterized by $(\sigma_{n,1}, \dots, \sigma_{n,E})$, and \mathbf{R}_k^t is a correlation matrix with the structure of exponential decay characterized by a scalar parameter $\rho_n \in (0, 1)$. Given $Z_n = 1$, where $n \in \{1, \dots, N\}$, we assume that $\boldsymbol{\xi}_{n,i,j,t}$ and $\boldsymbol{\varepsilon}_{n,i,j,e}$ are noise vectors generated by the new participant's parameters; Given $Z_n = 0$, we assume that $\boldsymbol{\xi}_{n,i,j,t}$ and $\boldsymbol{\varepsilon}_{n,i,j,e}$ are noise vectors generated by participant n 's parameters.

$$\begin{aligned}(\boldsymbol{\xi}_{n,i,j,t} \mid Z_n) &\sim \mathcal{MVN}\{\mathbf{0}, \boldsymbol{\Sigma}_0^s Z_n + \boldsymbol{\Sigma}_n^s (1 - Z_n)\}, \\ (\boldsymbol{\varepsilon}_{n,i,j,e} \mid Z_n) &\sim \mathcal{MVN}\{\mathbf{0}, \mathbf{R}_0^t Z_n + \mathbf{R}_n^t (1 - Z_n)\}.\end{aligned}\tag{4}$$

Let Θ be a collection of all unknown parameters. Our primary parameters of interest are those associated with the new participant, i.e., $\mathbf{B}_{0,1}$, $\mathbf{B}_{0,0}$, $\sigma_{0,e}^2$, η_0 , and ρ_0 , and posterior probability of matching indicators, i.e., $\Pr(Z_n = 1 \mid \mathbf{X}, \mathbf{Y})$, $n = 1, \dots, N$. The remaining parameters are considered as nuisance parameters.

3 Posterior Inferences

3.1 Model Reparametrization and Prior Specifications

We rewrite the model by applying the notation of matrix normal distribution

$$\begin{aligned}
 \mathbf{X}_{0,i,j} \mid Y_{0,i,j} = 1; \Theta &\sim \mathcal{MN}(\mathbf{B}_{0,1}, \Sigma_0^s, \mathbf{R}_0^t), \\
 \mathbf{X}_{0,i,j} \mid Y_{0,i,j} = 0; \Theta &\sim \mathcal{MN}(\mathbf{B}_{0,0}, \Sigma_0^s, \mathbf{R}_0^t), \\
 \mathbf{X}_{n,i,j} \mid Z_n, Y_{n,i,j} = 1; \Theta &\sim \mathcal{MN}\{\mathbf{B}_{0,1}Z_n + \mathbf{B}_{n,1}(1 - Z_n), \\
 &\quad \Sigma_0^s Z_n + \Sigma_n^s(1 - Z_n), \mathbf{R}_0^t Z_n + \mathbf{R}_n^t(1 - Z_n)\},
 \end{aligned} \tag{5}$$

where $\mathbf{B}_{n,1} = (\beta_{n,1,1}^\top, \dots, \beta_{n,1,E}^\top)$ ($n > 0$) and $\mathbf{B}_{0,0} = (\beta_{0,0,1}^\top, \dots, \beta_{0,0,E}^\top)$.

To better characterize the multi-channel ERP response functions $\{\mathbf{B}_{n,1}\}_{n=0}^N$ and $\mathbf{B}_{0,0}$, we frame them using the notation of a multivariate Gaussian process. First, we adopt the definition (Dixon and Crepey, 2018) to define a multivariate Gaussian processes as follows: Let $\boldsymbol{\mu} : \mathbb{R} \rightarrow \mathbb{R}^E$, $\kappa : \mathbb{R} \times \mathbb{R} \rightarrow \mathbb{R}$, $\boldsymbol{\Omega} \in \mathbb{R}^{E \times E}$, and $\{s_t\}_{t=1}^{T_0}$ be a vector-valued mean function, a kernel on the temporal domain, a positive definite parameter covariance matrix on the spatial domain, and input points, respectively. Here, the general multidimensional input vector is reduced to the scalar indexed by time only. \mathbf{f} is a multivariate Gaussian process on \mathbb{R} with vector-valued mean function $\boldsymbol{\mu}$, kernel κ , and row covariance matrix $\boldsymbol{\Omega}$ if the vectorization of any finite collection of vector-valued variables have a joint multivariate Gaussian distribution, i.e.,

$$\text{vec} \left\{ \left[\hat{\mathbf{f}}(s_1), \dots, \hat{\mathbf{f}}(s_{T_0}) \right] \right\} \sim \mathcal{MVN}(\text{vec} \{[\hat{\boldsymbol{\mu}}(s_1), \dots, \hat{\boldsymbol{\mu}}(s_{T_0})]\}, \boldsymbol{\Sigma} \otimes \boldsymbol{\Omega}), \tag{6}$$

where vec was the vectorization operator; $\hat{\mathbf{f}}(s), \hat{\boldsymbol{\mu}}(s) \in \mathbb{R}^E$ were column vectors that evaluated the functions \mathbf{f} and $\boldsymbol{\mu}$ at the index point s . Furthermore, $\boldsymbol{\Sigma} \in \mathbb{R}^{T_0 \times T_0}$ with $\Sigma_{t_1, t_2} = k(s_{t_1}, s_{t_2})$, where $t_1, t_2 \in \mathbb{Z}$ and $0 < t_1, t_2 \leq T_0$, and \otimes is the Kronecker product operator. We denote $\mathbf{f} \sim \mathcal{MGP}(\boldsymbol{\mu}, \kappa, \boldsymbol{\Omega})$.

In our case, we let $\mathbf{b}_{n,1}$ be an E -dim target ERP function of participant n characterized by $\boldsymbol{\mu}_{n,1}, \kappa_1, \boldsymbol{\Sigma}_n^s$, $n = 0, \dots, N$, and $\mathbf{b}_{0,0}$ be another E -dim non-target ERP function of participant 0 characterized by $\boldsymbol{\mu}_{0,0}, \kappa_0, \boldsymbol{\Sigma}_0^s$. To simplify, we let $\boldsymbol{\mu}_{n,1} = \boldsymbol{\mu}_{0,0} = \mathbf{0}$ and apply a γ -exponential kernel function to specify target kernel κ_1 and non-target kernel κ_0 as follows:

$$k(z_i, z_j) = \psi_0 \exp \left\{ - \left(\frac{\|z_i - z_j\|_2^2}{s_0} \right)^{\gamma_0} \right\}, \quad (7)$$

where $0 \leq \gamma_0 < 2, s_0 > 0$. In practice, γ_0 and s_0 are treated as hyper-parameters and selected among a group of values and we do not further differentiate among participants. For participant-specific kernel variance parameters $\psi_{n,1}$ and $\psi_{0,0}$, we assign Log-Normal priors with the a mean zero and a scale one. In addition, we define a function $\phi(\cdot)$ as an eigenfunction of kernel k with eigenvalue λ if it satisfies the following integral: $\int k(s, s')\phi(s)ds = \lambda\phi(s')$. In general, the number of eigenfunctions is infinite, i.e., $\{\phi_l(s)\}_{l=1}^{+\infty}$, and we rank them by the descending order of their corresponding eigenvalues $\{\lambda_l\}_{l=1}^{+\infty}$. The Mercer's Theorem suggests that the kernel function k can be decomposed as a weighted summation of normalized eigenfunctions $\phi_l(s)$ with positive eigenvalues λ_l and approximated with a sufficient large L subgroup as follows: $k(s, s') = \sum_{l=1}^{+\infty} \lambda_l \phi_l(s)\phi_l(s') \approx \sum_{l=1}^L \lambda_l \phi_l(s)\phi_l(s')$. Thus, a random function \mathbf{f} can be represented as a linear combination of the above eigenfunctions and approximated with a sufficient large L subgroup evaluated at s as follows:

$$\mathbf{f}(s) = \begin{pmatrix} f_1(s) \\ \vdots \\ f_E(s) \end{pmatrix} = \begin{pmatrix} \sum_{l=1}^{\infty} a_{1,l}\phi_l(s) \\ \vdots \\ \sum_{l=1}^{\infty} a_{E,l}\phi_l(s) \end{pmatrix} \approx \begin{pmatrix} \sum_{l=1}^L a_{1,l}\phi_l(s) \\ \vdots \\ \sum_{l=1}^L a_{E,l}\phi_l(s) \end{pmatrix},$$

where $(a_{1,l}, \dots, a_{E,l})^\top \sim \mathcal{MVN}(\mathbf{0}, \boldsymbol{\Omega}), l > 0$. For participant-and-channel-specific noise variance parameters $\sigma_{n,e}^2$, we assign Half-Cauchy priors with a mean zero and a scale five. For temporal and spatial parameters ρ_n and η_n , we assign discrete uniform priors among a

grid of candidate values between 0 and 1. For $n = 0, \dots, N, e = 1, \dots, E$,

$$\begin{aligned} \mathbf{b}_{n,1}(s) &\sim \mathcal{MG}\mathcal{P}(\mathbf{0}, \psi_{n,1}\kappa_1, \Sigma_n^s), & \mathbf{b}_{0,0}(s) &\sim \mathcal{MG}\mathcal{P}(\mathbf{0}, \psi_{0,0}\kappa_0, \Sigma_0^s), \\ \psi_{n,1}, \psi_{0,0} &\stackrel{\text{indep.}}{\sim} \mathcal{LN}(0, 1), & \sigma_{n,e} &\sim \mathcal{HC}(0, 5.0), & \rho_n &\sim \mathcal{U}(0, 1), & \eta_n &\sim \mathcal{U}(0, 1), \end{aligned} \quad (8)$$

3.2 Markov Chain Monte Carlo

We apply the Gibbs Sampling method to estimate random functions $\mathbf{b}_{n,1}, \mathbf{b}_{0,0}$ and covariance-related parameters $\sigma_{n,e}^2, \rho_n$, and η_n . By Mercer's representation theorem, we obtain that

$$\begin{aligned} \mathbf{b}_{n,1}(s) &= \psi_{n,1} \sum_{l=1}^{+\infty} \text{Diag}(\mathbf{a}_{n,1,l}) \phi_{1,l}(s) \approx \psi_{n,1} \sum_{l=1}^{L_1} \text{Diag}(\mathbf{a}_{n,1,l}) \phi_{1,l}(s), & n = 0, \dots, N, \\ \mathbf{b}_{0,0}(s) &= \psi_{0,0} \sum_{l=1}^{+\infty} \text{Diag}(\mathbf{a}_{0,0,l}) \phi_{0,l}(s) \approx \psi_{0,0} \sum_{l=1}^{L_0} \text{Diag}(\mathbf{a}_{0,0,l}) \phi_{0,l}(s), \end{aligned} \quad (9)$$

where $\{\mathbf{a}_{n,1,l}\}_{n=0}^N$ and $\mathbf{a}_{0,0,l}$ are column vectors of coefficient parameters associated with eigenfunctions $\phi_{1,l}$ and $\phi_{0,l}$, respectively. We evaluate $\mathbf{b}_{n,1}(s)$ and $\mathbf{b}_{0,0}(s)$ over a group of input time points $\{s_t\}_{t=1}^{T_0}$ and define them $\mathbf{B}_{n,1}$ and $\mathbf{B}_{0,0}$, respectively. Then, we adopt Eq (7) to calculate the kernel covariances Ψ_1 and Ψ_0 associated with kernel function κ_1 and κ_0 , respectively. $\mathbf{B}_{n,1}$ and $\mathbf{B}_{0,0}$ can be approximated by

$$\begin{aligned} \mathbf{B}_{n,1} &\approx \psi_{n,1} \cdot \mathbf{A}_{n,1} \Psi_1^{1:L_1}, & \mathbf{A}_{n,1} &= (\mathbf{a}_{n,1,1} \cdots \mathbf{a}_{n,1,l} \cdots \mathbf{a}_{n,1,L_1}), & n \in \{0, \dots, N\}, \\ \mathbf{B}_{0,0} &\approx \psi_{0,0} \cdot \mathbf{A}_{0,0} \Psi_0^{1:L_0}, & \mathbf{A}_{0,0} &= (\mathbf{a}_{0,0,1} \cdots \mathbf{a}_{0,0,l} \cdots \mathbf{a}_{0,0,L_0}), \\ \mathbf{A}_{n,1} &\sim \mathcal{MN}(\mathbf{0}, \Sigma_n^s, \mathbf{V}_{\Psi_1}^{1:L_1}), & \mathbf{A}_{0,0} &\sim \mathcal{MN}(\mathbf{0}, \Sigma_0^s, \mathbf{V}_{\Psi_0}^{1:L_0}), \end{aligned} \quad (10)$$

where $\mathbf{A}_{n,1}$ and $\mathbf{A}_{0,0}$ follow matrix normal prior distributions with closed posterior forms (Zhang et al., 2021), and $\Psi_1^{1:L_1}, \Psi_0^{1:L_0}, \mathbf{V}_{\Psi_1}^{1:L_1}$, and $\mathbf{V}_{\Psi_0}^{1:L_0}$ are the first L_1 rows of Ψ_1 , the first L_0 rows of Ψ_0 , the diagonal matrix of the first L_1 eigenvalues associated with Ψ_1 , and the diagonal matrix of the first L_0 eigenvalues associated with Ψ_0 , respectively. In practice, L_1 and L_0 are determined by the minimum integer of which cumulative sum of eigenvalues divided by the total sum of eigenvalues is over 95% after reordering them by the descending order. For the remaining parameters, we apply Metropolis-Hastings algorithm

to draw posterior samples. For the convergence check, we run multiple chains with different seed values and evaluate the convergence by Gelman-Rubin statistic (Gelman and Rubin, 1992). In addition, we examine the chain-specific posterior means of $\{Z_n\}$ as a post-hoc way to demonstrate the convergence. Details of MCMC implementations can be found in the supplementary material.

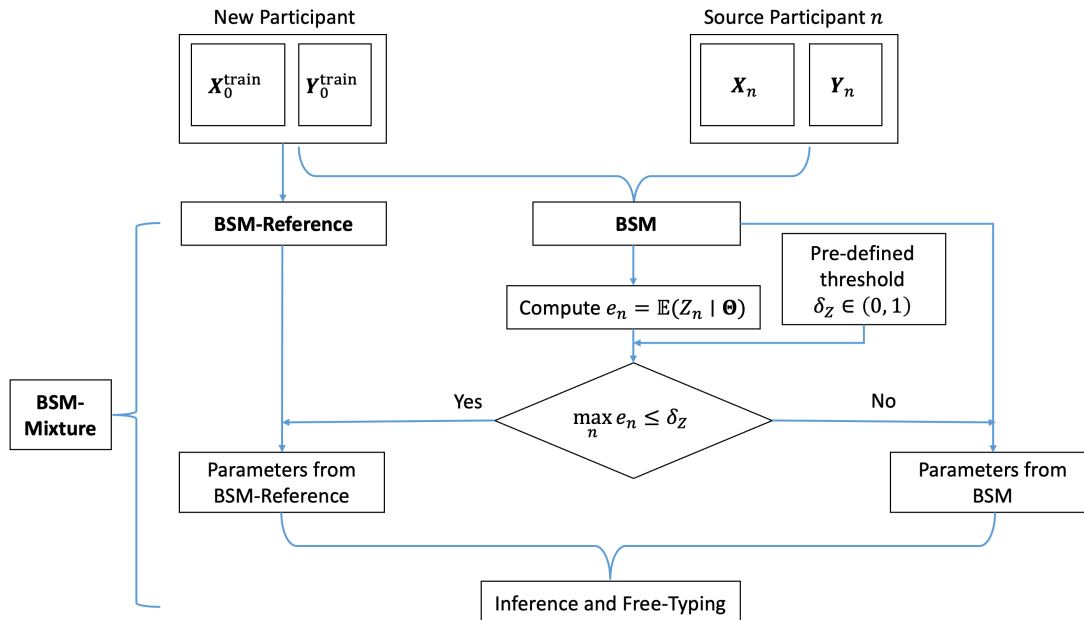


Figure 2: An illustration of the BSM-Mixture algorithm. First, we pre-define a threshold $\delta_Z \in (0, 1)$. Second, we fit BSM model and obtain posterior samples of $\{Z_n\}$ to compute $\mathbb{E}(Z_n | \Theta)$. If none of the posterior expectations exceed δ_Z , we apply BSM-Reference, otherwise, we apply BSM model for prediction. Note that both BSM-Reference and BSM models can be fitted simultaneously, and it will not have extra computational burden to the total calibration effort.

3.3 Hybrid Model Selection Strategy: BSM-Mixture

Since our primary goal is to use small amount of training data from the new participant for calibration data, it may be challenging for our BSM model to identify source participants when no source participants are available for matching. In practice, we propose the hybrid

model selection strategy, namely **BSM-Mixture**, such that if no source participants were selected satisfying certain threshold, we would use BSM-Reference for prediction. We define the hybrid model selection strategy as follows: First, we pre-define a threshold $\delta_Z \in (0, 1)$. Second, we fit BSM model and obtain the posterior samples of $\{Z_n\}$ to compute $\mathbb{E}(Z_n | \Theta)$. If none of $\mathbb{E}(Z_n | \Theta)$ exceed δ_Z , we apply BSM-Reference, otherwise, we apply BSM model for prediction. Note that BSM-Reference and BSM model can be fitted simultaneously, it does not add much computational burden to the total calibration effort. In addition, since the current data have been collected from the single lab source, we do not expect to see significant impact of machine effect on the parameter estimation and prediction accuracy. Figure 2 provides an illustration of the hybrid model selection strategy on BSM-Mixture.

3.4 Posterior Character-Level Prediction

One of the advantages of our method is to predict on testing data directly without refitting the data. Under the RCP design, the character-level prediction depends on selecting the correct row and column within each sequence. Let \mathbf{W}, \mathbf{Y} , and \mathbf{X} be existing stimulus-code indicators, stimulus-type indicators, and matrix-wise EEG signals, respectively. Let $\mathbf{W}_0^*, \mathbf{Y}_0^*, \mathbf{X}_0^*$, and Θ_0 be additional one sequence of stimulus-code indicators, stimulus-type indicators, matrix-wise EEG signals, and the parameter set, respectively, associated with the new participant. To simplify the notation, we assume that the new participant is spelling the same target character ω . Based on the property described in Section 2.1, let \mathbf{y}_ω^* be the possible values of stimulus-type indicators given \mathbf{W}_0^* and the target character ω .

$$\Pr(\mathbf{Y}_0^* = \mathbf{y}_\omega^* | \mathbf{X}_0^*, \mathbf{W}_0^*, \mathbf{X}, \mathbf{W}, \mathbf{Y}) = \int \Pr(\mathbf{Y}_0^* = \mathbf{y}_\omega^* | \Theta_0; \mathbf{X}_0^*, \mathbf{W}_0^*) \Pr(\Theta_0 | \mathbf{X}, \mathbf{W}, \mathbf{Y}) d\Theta_0,$$

$$\Pr(\mathbf{Y}_0^* = \mathbf{y}_\omega^* | \Theta_0; \mathbf{X}_0^*, \mathbf{W}_0^*) \propto \underbrace{\Pr(\mathbf{X}_0^* | \Theta_0; \mathbf{W}_0^*, \omega)}_{\text{Equation (5)}} \cdot \Pr(\omega \text{ is target}),$$
(11)

Here, $\Pr(\omega \text{ is target}) = 1/36$ is the predictive prior on each candidate character with non-informative priors under the RCP design. When we need multiple sequence replications to select the target character, we modify the above formula by multiplying the sequence-specific posterior conditional likelihood within each cluster.

4 Simulation Studies

We conduct extensive simulation studies to demonstrate the advantage of our proposed framework. We show the results of two simulation scenarios: a naive multi-channel setting and a real data based setting.

4.1 Naive Multi-channel Simulation Scenario

Setup We consider the scenario with $N = 7$ and $K = 3$. The simulated EEG signals are generated from multivariate normal distributions with a response window of 35 time points per channel, i.e., $T_0 = 35$. We design three groups of parameters including two-dimensional pre-specify mean ERP functions and variance nuisance parameters, where the shape and magnitude parameters are based on real participants from the database (Thompson et al., 2014). For simulated data generated from group 0, we create a typical P300 pattern for the first channel where the target ERP function reach its positive peak around 10th time point post stimulus and reverse the sign for both ERP functions for the second channel; for simulated data generated from group 1, we create the same target ERP function as group 0 for the first channel and reduce the peak magnitude for the second channel; for simulated data generated from group 2, we reduce the peak magnitude for the first channel and create the same ERP functions as group 1 for the second channel. We consider an autoregressive temporal structure of order 1 (i.e., AR(1)), compound symmetry spatial structure, and channel-specific variances for background noises, where the true parameters for groups 0,

1, and 2 are $(\rho_0 = 0.7, \eta_0 = 0.6, \sigma_{0,1} = 8.0, \sigma_{0,2} = 8.0)$, $(\rho_1 = 0.7, \eta_1 = 0.4, \sigma_{1,1} = 8.0, \sigma_{1,2} = 6.0)$, and $(\rho_2 = 0.5, \eta_2 = 0.4, \sigma_{2,1} = 2.0, \sigma_{2,2} = 2.0)$, respectively. We design two cases for this scenario, a case without matched data among source participants (Case 1) and a case with matched data (Case 2). For Case 1, the group labels for source participants 1-6 are 1, 1, 2, 2, and 2, respectively. For Case 2, the group labels for source participants 1-6 were 0, 0, 1, 1, 2, and 2, respectively. We perform 100 replications for each case. Within each replication, we assume that each participant is spelling the character “T” three times with ten sequence replications per character for training and generate additional testing data of the same size as the testing data of the single-channel scenario.

Settings and Diagnostics All simulated datasets are fitted with equation (5). We also apply two covariance kernels κ_1 and κ_0 for target and non-target ERP functions, respectively. The two kernels are characterized by γ -exponential kernels with length-scale and gamma hyper-parameters as $(0.2, 1.2)$ and $(0.3, 1.2)$, respectively. The pre-specified threshold δ_Z is 0.5. We run the MCMC with three chains, with each chain containing 5,000 burn-ins and 3,000 MCMC samples.

Criteria We evaluate our method by matching and prediction. For matching, we report the proportion that each source participant is matched to the new participant and produce the ERP function estimates with 95% credible bands with respect to the training sequence size. For prediction, we report the character-level prediction accuracy of the testing data, using Bayesian signal matching with source participants’ data (BSM), Bayesian generative methods with the new participant’s data only (BSM-Reference), the hybrid model selection strategy (BSM-Mixture), an existing classification method with data borrowing using Riemannian Geometry (MWDM), and swLDA with new participant’s data only (swLDA). We do not include SMGP for comparison in the simulation studies because SMGP assumes that data are generated under sequences of stimuli, while our data generative mechanism is based on stimuli. We does not include other conventional ML methods because the

Table 1: The **upper** and **lower** panels show summary of means and standard deviations of $Z_n = 1$ for Cases 1 and 2 across 100 replications by BSM, respectively. The numerical values are multiplied by 100 for convenience and were reported with respect to the training sequence replications.

Participant ID	Sequence Size									
	1	2	3	4	5	6	7	8	9	10
1	31.7, 25.6	14.3, 18.5	8.2, 13.6	9.1, 14.8	8.7, 14.6	7.2, 13.7	7.9, 14.0	8.8, 15.4	8.2, 15.1	7.8, 13.2
2	28.5, 26.3	15.3, 19.8	9.8, 16.6	9.5, 17.0	9.8, 16.6	7.5, 15.4	8.1, 13.6	6.8, 12.5	8.8, 14.0	9.2, 14.9
3	32.8, 26.2	15.3, 19.3	9.2, 15.0	11.4, 17.2	8.9, 14.7	9, 15.7	11.1, 17.1	7.2, 13.7	6.5, 12.3	9.4, 15.8
4	1.3, 3.3	1.6, 4.5	1.1, 0.3	1.4, 3.3	0.9, 0.3	0.9, 0.3	1.3, 3.3	1.0, 0.3	1.0, 0.3	1.7, 4.6
5	2.3, 6.4	1.4, 3.3	1.7, 4.6	2.3, 6.4	1.0, 0.3	1.0, 0.3	1.0, 0.3	1.6, 4.6	2.0, 5.7	1.3, 3.2
6	1.0, 0.4	1.0, 0.3	1.7, 4.6	1.0, 0.3	1.7, 4.6	1.3, 3.3	1.3, 3.2	1.7, 4.6	1.3, 3.3	2.0, 5.6

Participant ID	Sequence Size									
	1	2	3	4	5	6	7	8	9	10
1	75.9, 22.9	83.0, 20.0	89.0, 16.0	87.8, 17.9	92.3, 13.3	92.5, 14.1	92.2, 15.0	92.9, 13.2	93.3, 11.4	93.2, 13.4
2	76.5, 22.0	81.0, 21.4	87.9, 17.6	87.3, 18.7	92.6, 14.2	91.2, 16.5	92.2, 14.1	91.8, 14.8	91.6, 15.2	91.2, 14.1
3	15.5, 19.7	10.0, 14.5	12.4, 17.5	8.2, 15.1	6.6, 12.3	10.0, 15.4	6.9, 13.4	4.3, 10.9	6.8, 14.1	7.9, 14.1
4	12.1, 18.0	11.7, 15.4	12.1, 18.6	9.2, 16.5	9.1, 16.3	7.5, 13.1	9.0, 15.5	8.2, 14.3	7.8, 14.8	6.5, 12.3
5	1.7, 4.5	1.0, 0.3	1.0, 0.4	1.3, 3.3	1.0, 0.3	1.0, 0.3	1.6, 4.6	2.0, 5.6	1.3, 3.3	1.0, 0.3
6	1.4, 3.3	1.0, 0.3	1.3, 3.3	1.3, 3.2	1.0, 0.3	1.1, 0.3	1.0, 0.3	0.9, 0.3	1.0, 0.3	1.0, 0.4

prediction accuracy of swLDA is representative of those types of methods.

Matching Results The upper and lower panels of Table 1 show the means and standard deviations of $Z_n = 1$ across 100 replications for cases without and with matched data, respectively, by BSM. The numerical values are multiplied by 100 for convenient reading and are reported with respect to the training sequence size of the new participant. For Case 1, all the values quickly drop below 10.0 with 3 training sequence replications; for Case 2, values associated with Participants 1-2 are above 75.0 across all the training sequences and values associated with Participants 3-6 quickly drop below 10.0 within 4 sequence replications. The results indicate that our method correctly perform the participant selection.

Prediction Results The left and right panels of Figure 3 show the means and standard errors of testing prediction accuracy of Case 1 (No Matched) and Case 2 (Matched) by BSM-Mixture, BSM, BSM-Reference, MDWM, and swLDA, respectively. The testing prediction accuracy is further stratified by training the first 2, 3, and 4 sequences of the

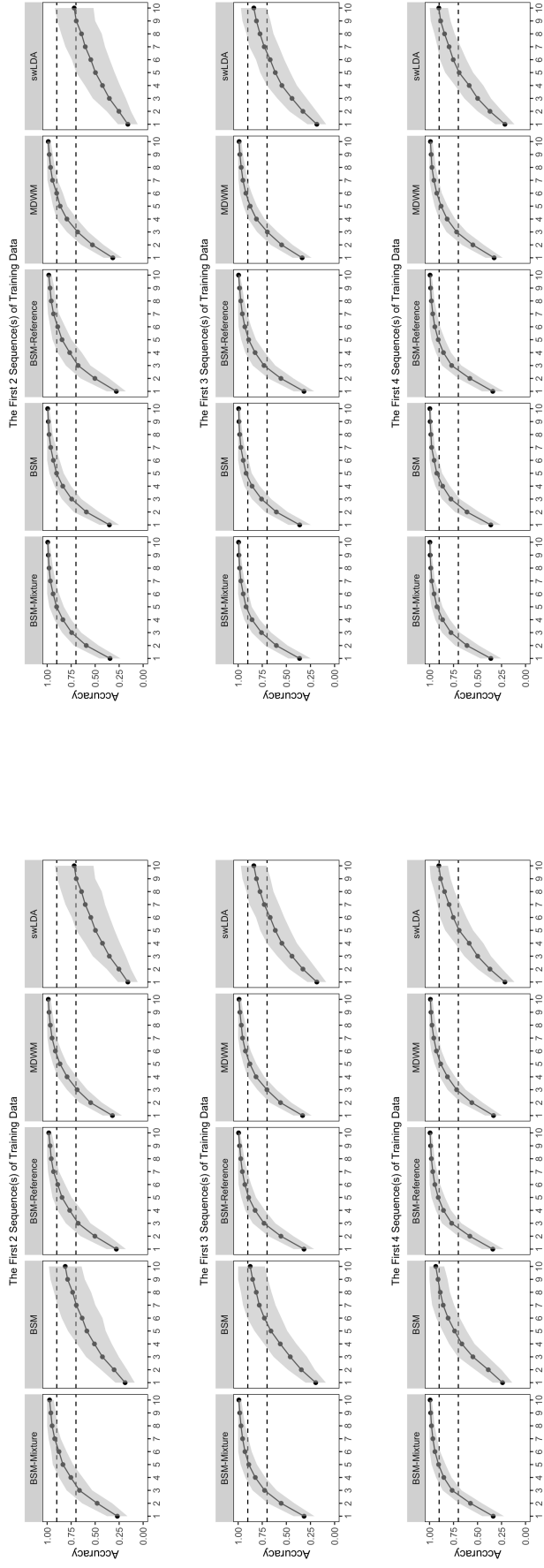


Figure 3: The **left** and **right** panels show the means and standard errors of testing prediction accuracy of Cases 1 (Unmatched) and 2 (Matched) by BSM-Mixture, BSM, BSM-Reference, MDWM, and swLDA across 100 replications, respectively. The upper, middle, and lower panels show prediction accuracy with the first 2, 3, and 4 training sequence replications, respectively. For Unmatched scenarios, BSM-Mixture was robust to source participants by adopting BSM-Reference’s results, while for Matched scenario, BSM-Mixture required one testing sequence fewer than BSM-Reference to achieve the 90% threshold with narrower error bars.

new participant. For Case 1, within the same row, BSM-Mixture and BSM-Reference have similar performances to MDWM. The poor performance of BSM is due to the uncertainty among participant selection in presence of no source participant and small training sample size. Therefore, the hybrid model selection strategy solves this issue. For Case 2, within the same row, BSM-Mixture performs the best, followed by MDWM, suggesting that our method successfully identifies the matched participants and leverages their information correctly. Within the same column, four methods benefit from an increasing number of training data from the new participant.

4.2 Real Data Based Simulation Scenario

We design a real-data based multi-channel simulation scenario. True parameters and sample sizes of training sets are copied from the real data analysis. We follow the tradition that participant 0 refers to the new participant, while participants 1 to 23 refer to the source participants. The participant-specific mean ERP functions and variance nuisance parameters are obtained from posterior means of each participant in the real data analysis. We multiply the variance estimates by 2 in this simulation scenario. The simulated EEG signals are also generated from multivariate normal distributions with a response window of 25 time points per channel, i.e., $T_0 = 25$. We perform 100 replications for this scenario. Within each replication, we assume that each participant is spelling the character “T” eight times with ten sequence replications per character for training and generate additional testing data of the same size as the testing data of the naive multi-channel scenario. All simulated datasets are fitted with equation (5). We used the same kernels, hyper-parameters, and the threshold δ_Z as the real data analysis. We run the MCMC with three chains, with each chain containing 5,000 burn-ins and 3,000 MCMC samples. Both matching and prediction results are reported, and we follow the same criteria as mentioned in Section 4.1.

Results For matching, we only observe that participant 1 has a posterior mean of being

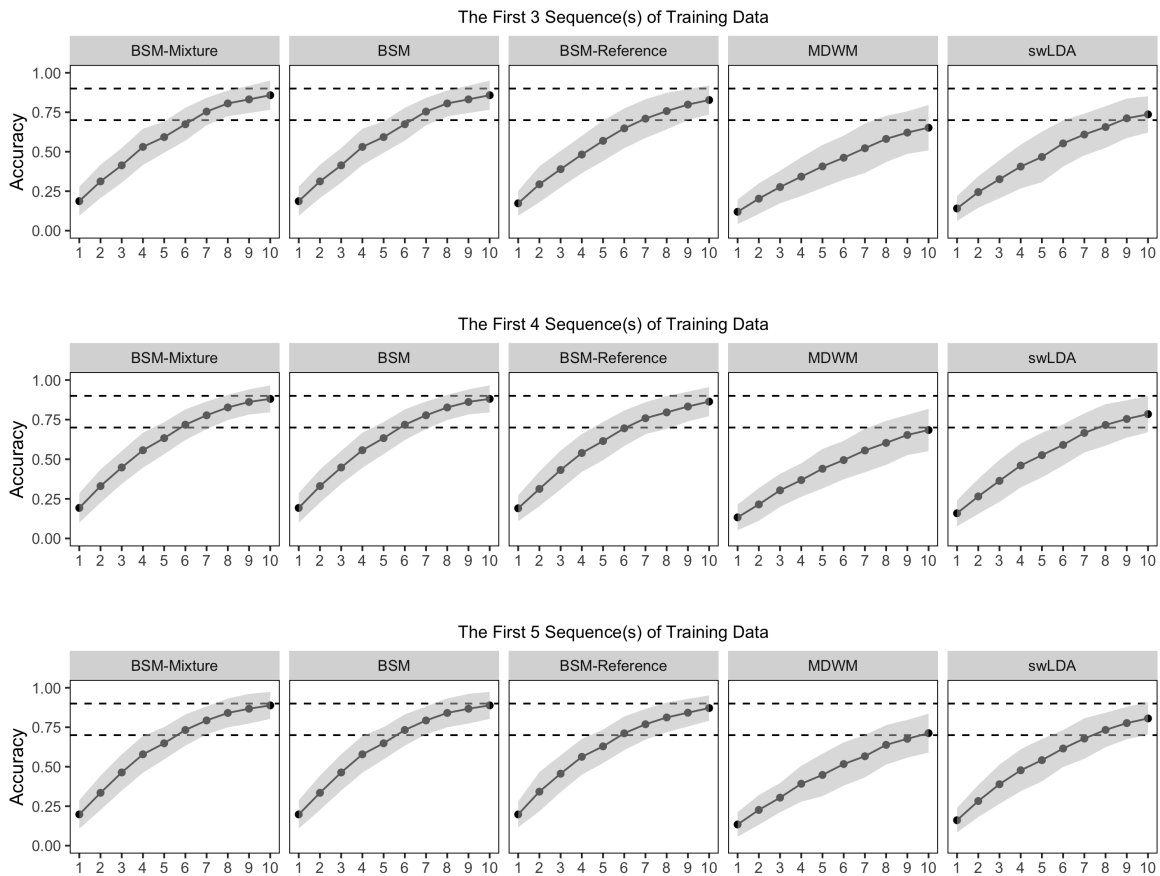


Figure 4: A graphic of the testing prediction accuracy. The upper, middle, and lower panel corresponds to the prediction accuracy with the first 3, 4, and 5 sequences of training data, respectively. All results are evaluated across 100 replications.

merged around 0.2, while the posterior means of other source participants are below 0.1. The finding is consistent with the matching from the real data analysis given the same participant ordering and supports our argument that we typically expect one or two matching based on BSM classifier. Details of selection probability can be found in Section S4.2 in the supplementary. For prediction, Figure 4 shows the testing prediction accuracy by the same five methods across 100 replications. The upper, middle, and lower panels are the prediction accuracy by training the first 2, 3, and 4 training sequences of the new participant. Overall, we observe that BSM-Mixture performs better than MDWM and swLDA. The prediction curves of BSM-Mixture and BSM are almost identical, suggesting that the al-

gorithm identifies at least one source participant with the posterior mean of being merged exceeds the threshold $\delta_Z = 0.1$, which is also consistent with the matching result. The prediction accuracy of BSM is slightly higher and narrower than that of BSM-Reference, possibly because the borrowing information may be limited when only one participant has reached the selection threshold. Finally, when we increase the sample size of training data, the prediction accuracy improves accordingly.

5 Analysis of BCI data from Real Participants

We examine the performance of our BSM framework on real-participant data, where the real data were originally collected from the University of Michigan Direct Brain Interface Laboratory (UMDBI). A total of 41 participants were recruited to accomplish the experiment, and we demonstrated the results of nine participants with brain damages or neuro-degenerative diseases. Each participant completed one calibration (training) session (TRN) and up to three free-typing sessions (FRT). For the calibration session, each participant was asked to copy a 19-character phrase “THE_QUICK_BROWN_FOX” including three spaces with 15 sequences, while wearing an EEG cap with 16 channels and sitting close to a monitor with a virtual keyboard with a 6×6 grid. Details of the experimental setup can be found Thompson et al. (2014).

The steps of the real data analysis are outlined as follows: First, we performed pre-processing techniques on raw EEG signals. Next, we identified a proper source participant pool based on testing swLDA accuracy. We trained swLDA and SMGP as two reference methods using the calibration data from the new participant only and trained BSM-Mixture and MDWM as two methods with data borrowing. The swLDA method was an existing efficient classifier. The MDWM method simply identified common features between the new participant and each source participant and did not perform explicit participant se-

lection. Note that the SMGP method primarily focused on detecting the spatial-temporal discrepancies on brain activity between target and non-target ERP functions under the sequence-based analysis framework, while the other three methods treated stimulus-specific EEG data as feature vectors for classification. We did not include other conventional ML methods because they did not have the borrowing version. We demonstrated the detailed results of Participant K151, a senior male diagnosed with amyotrophic lateral sclerosis (ALS), and showed the results of remaining participants in the supplementary materials.

5.1 Data Pre-processing Procedure and Model Fitting

We applied the band-pass filter between 0.5 Hz and 6 Hz and down-sampled the EEG signals with a decimation factor of 8. Next, we extracted a fixed response window of approximately 800 ms after each event such that the resulting EEG matrix contained 15 sequence segments, and each sequence contained 12 extracted event-related EEG signal segments. The resulting event-related EEG signal segment had around 800 ms, i.e., 25 sampling points per channel. Since the SNR of EEG signals is typically low, we further applied the xDAWN filter to enhance the evoked potentials (Rivet et al., 2009). The xDAWN method was an unsupervised algorithm that decomposed the raw EEG signals into relevant P300 ERPs and background noises and aimed to find a robust spatial filter that projected raw EEG signal segments onto the estimated P300 subspace by *directly* modeling noise in the objective function. We used all 16 channels as the signal input and selected the first two major components. We will denote raw EEG signal inputs and ERP functions after the xDAWN algorithm as transformed EEG signals and transformed ERP functions, respectively.

To emphasize the calibration-less point, we used a small portion of K151’s training set and abundant training set from source participants. We identified 23 participants whose prediction accuracy of swLDA on FRT files exceeded 50% and used them as the

source participant pool: For each source participant, we included the first 10 sequence replications of the first five characters: “THE_Q”, and the testing prediction accuracy was obtained with all FRT files (up to three sessions per participant). For K151, we included the first five sequence replications of the same five characters. Therefore, the resulting EEG feature matrices for the new participant and source participants had sizes of (300, 2, 25) and (600, 2, 25), respectively. Here, 300, 600, 2, and 25 were the number of stimuli for new participant, the number of stimuli for source participants, the number of transformed ERP components and the length of EEG response window, respectively.

The datasets were fitted with the equation (5). We applied two covariance kernels κ_1 and κ_0 for target and non-target ERP functions, respectively. Two kernels were characterized by γ -exponential kernels with length-scale and gamma hyper-parameters as (0.2, 1.2) and (0.3, 1.2), respectively. We ran the MCMC with three chains, with each chain containing 8,000 burn-ins and 1,000 MCMC samples. The Gelman-Rubin statistics were computed to evaluate the convergence status of each model. For matching, we reported the selection indicator Z_n . Due to the data heterogeneity, we expect to see partial matching. The largest posterior mean of $\{Z_n\}$ is around 0.2, the δ_Z should not exceed 0.2. In addition, most posterior means are around 4%, and we expect to see two or three source participants to match with the new participant. We set the $\delta_Z = 0.1$, i.e., the mean of 2/24 and 3/24. We also produced the transformed EEG signal function estimates by BSM and compared them to the results by BSM-Reference. For prediction, we reported the prediction accuracy on FRT files by BSM-Mixture, MDWM, swLDA, and SMGP up to five testing sequences. We only reported BSM-Mixture to utilize both advantages of BSM and BSM-Reference.

5.2 Inference and Prediction Results

For the estimation of mean-level transformed signals, Figure 5 shows the inference results of K151. The first columns show the mean estimates and their 95% credible bands of the

first two transformed ERP functions by BSM-Mixture. Only target ERP information was borrowed. The middle and right columns show the spatial pattern and spatial filter of the new participant’s partial training data by xDAWN, respectively.

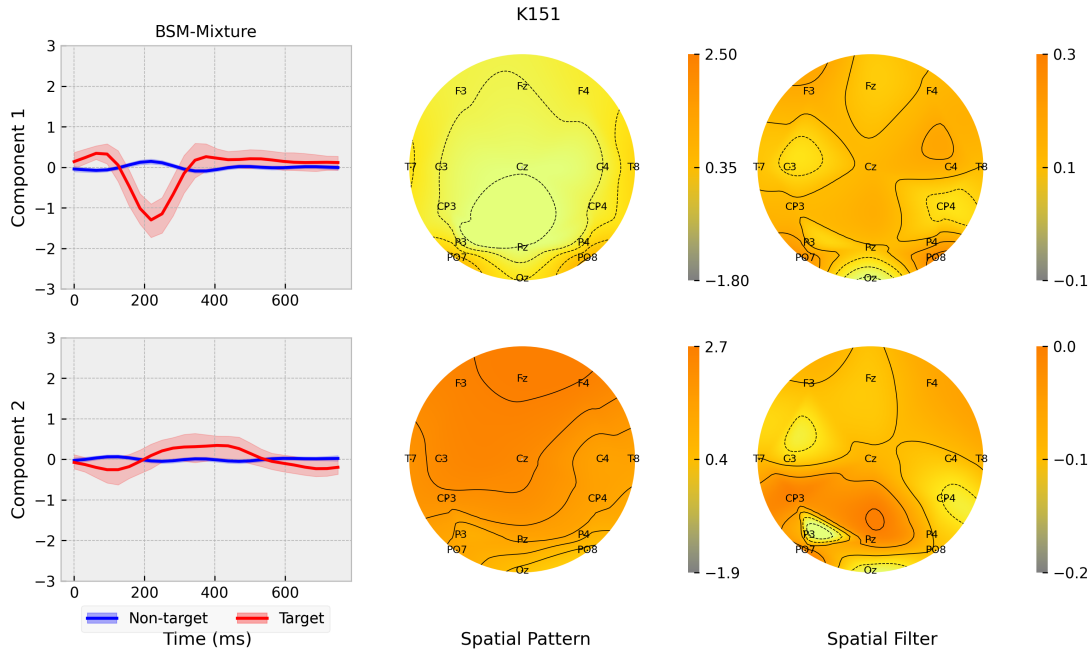


Figure 5: The first column shows the mean estimates with 95% credible bands of the first two transformed ERP functions by BSM-Mixture. Only target ERP information is borrowed. The middle and right columns show the spatial patterns and spatial filters of the new participant’s partial training data by xDAWN, respectively.

For Component 1, we observed a sinusoidal pattern such that the transformed ERP response achieved a minor positive peak around 50 ms post stimulus and a major negative peak around 200 ms post stimulus. The signal achieved its second positive peak around 350 ms post stimulus and gradually decreased to zero. Spatial pattern and filter plots indicated that the major negative peak was primarily attributed to parietal-occipital and occipital regions (channels PO7, PO8, and Oz). For Component 2, we observed a Mexican-hat pattern with a double-camel-hump feature. The transformed target ERP response achieved its first negative peak around 100 ms post stimulus and its two positive peaks around 250

ms and 450 ms post stimulus before it gradually decreased to zero. Spatial pattern and filter plots indicated that such double-positive peak might be associated with the signals in central and parietal regions. The credible bands of BSM-Mixture were generally wider than BSM-Reference due to the uncertainty of pairwise comparisons among source participants.

For matching results, based on the P300 ERP estimation from BSM-Reference, we expect one or two source participants to match with the new participant, so we set the prior probability of $Z_n = 1$ as $\Pr\{Z_n = 1\} = 2/24 \approx 8\%$. And we set the δ_Z to be slightly higher than the prior probability, i.e., 10%. Among 23 source participants, five source participants had posterior probability of being merged with K151 greater than or equal to 10%. Of all, K111 showed the greatest similarity to K151, with a posterior probability of 25%, followed by K158 (16%), K183 (15%), and K172 (13%). The mean and median values of posterior probability $\Pr\{Z_n = 1\}$ were 6.4% and 4.0%, respectively. Details of the matching results can be found in the Section S5.2 in the Supplementary material. Given the general low signal-to-noise ratio in EEG data, our borrowing results based on mean-level separation effects were not dominated by any particular source participant.

Table 2: Prediction accuracy (percentage) of all FRT files with up to six testing sequences by BSM-Mixture, MDWM, swLDA, and SMGP with five training sequences.

Testing Sequence Size	Borrowing Methods		Reference Methods	
	BSM-Mixture	MDWM	swLDA	SMGP
1	54.1%	47.3%	37.8%	16.2%
2	82.4%	71.6%	50.0%	23.0%
3	83.8%	75.7%	67.6%	40.5%
4	89.2%	81.1%	75.7%	39.2%
5	90.5%	90.5%	81.1%	51.4%
6	94.6%	95.9%	83.8%	59.8%

Table 2 shows the total prediction accuracy of all FRT files with respect to the testing

sequences up to six by BSM-Mixture, MDWM, swLDA, and SMGP with five training sequences for K151. Overall, BSM-Mixture performed better than two reference methods. BSM-Mixture achieves an 85.1% accuracy within 2 testing sequences, which is slightly faster than the existing method MDWM. Unfortunately, the SMGP method performs poorly in this case due to different assumptions in the analysis framework. The SMGP method treats one sequence of EEG data as an analysis unit, while our BSM framework treats one stimulus of EEG data as an analysis unit. Therefore, under the RCP design, the sample size for SMGP is 1/12 of that for BSM-Mixture, which leads to inaccurate estimation of P300 response functions and poor prediction on FRT files.

In general, the advantage of BSM-Mixture is reflected in later testing sequences when participants are more likely to get distracted and have a higher heterogeneity level of EEG signals over time. Certain temporal intervals may become less separable and the attenuated amplitude estimates on these potentially confusing regions by BSM-Mixture actually reduce the negative effect of growing signal heterogeneity on prediction accuracy. For K151, temporal regions such as [500 ms, 800 ms] of Component 1, the double peaks of Component 2 by BSM-Mixture are both attenuated than those by BSM-Reference. However, that the initial 100 ms and intervals around 350 ms of Component 1 becomes even more separable by BSM-Mixture may suggest that those intervals are robust over time and essential to maintain high prediction accuracy during FRT tasks.

6 Discussion

In this article, we propose a hierarchical Bayesian Signal Matching (BSM) framework to build a participant-semi-dependent, calibration-less framework with applications to P300 ERP-based Brain-Computer Interfaces. The BSM framework reduces the sample size for calibration of the new participant by borrowing data from pre-existing source partici-

pants’ pool at the participant level. The BSM framework specifies the joint distribution of stimulus-related EEG signal inputs via a Bayesian hierarchical mixture model. Unlike conventional clustering approaches, our method specifies the baseline cluster associated with the new participant and conducts pairwise comparisons between each source participant and the new participant by the criterion of log-likelihood. In this way, our method avoids the cluster label switching issue and can pre-compute model parameters from source participants to speed up the calibration. In addition, since our method intrinsically borrows the information from source participants via the binary selection indicators, we can use parameters from the baseline cluster to test directly without refitting the model with the augmented data. Finally, our hierarchical framework is base-model-free, such that it can be extended to any other classifiers with clear likelihood functions. We demonstrate the advantages of our method using extensive single- and multi-channel simulation studies and focus on the cohort with brain damages.

In the real data analysis, we find that first transformed ERP response is associated with the effect of visual cortex (higher positive values within parietal-occipital and occipital regions, while close to zero elsewhere) and that the second transformed ERP response is associated with the typical P300 responses (higher positive values within central and parietal regions). The resulting pattern with double-camel humps may be due to the effect of latency jitter (Guy et al., 2021) or simply the superimposed effect of various signal contributions from central and parietal electrodes by xDAWN. The cross-participant results also suggest that major negative peaks before 200 ms and positive peaks around 350 ms post stimulus are preserved in the first two transformed ERP responses. The above scientific findings are consistent with the finding from our previous study Ma et al. (2022) that the performance of the P300 speller greatly depends on the effect of the visual cortex, in addition to electrodes located in central and parietal regions.

In addition, compared to the simulation studies, the borrowing results of the real data

analysis show partial matching. Several reasons accounted for the results: First, the data generation mechanism of our method assumed that each observed EEG signal input is generated independently across stimuli, while the real data were extracted with overlapping EEG components between adjacent stimuli, and the overlapping temporal features still exist after applying the xDAWN filter. It is a potential model mis-specification to apply our method to the real data, which might make it difficult to find a very good match on the participant level. Second, our similarity criterion is based on calculating the log-likelihood of the target transformed ERP functions using the generative base classifier, which may be more sensitive to noise than discriminant classifiers. In simulation studies, the noises are clearly defined and well controlled. In the real data analysis, the noises may not be normally distributed, and the heterogeneity level of data increases not only across participants but also within the same participant over time, and the growing variability of data tends to compromise the separation effects of transformed ERPs. Fortunately, since BSM models the selection indicator in a soft-threshold manner, it has a flavor of Bayesian averaging that generally attenuates the magnitudes of peaks. Such diminishing differences between target and non-target transformed ERP function estimates suppress the weights of “ambiguous” temporal intervals and reduce the negative impact of false positives.

For cross-participant analysis, although we acknowledge the difference among the large and diverse source population, the features of interests for task-based, P300 ERP speller system are more consistent and easier to identify, compared to resting-state EEG data. We argue that the similarity exists among the participants who use this application. The transformed ERP function estimates of BSM are consistently attenuated compared to BSM-Reference, and the patterns of first two components are similar across nine participants. Figure 6 demonstrates the prediction accuracy of our target population cohort by BSM-Mixture, MDWM, swLDA, and SMGP. BSM-Mixture has similar prediction accuracy to MDWM, and they perform better than two reference methods. The minimal useful ac-

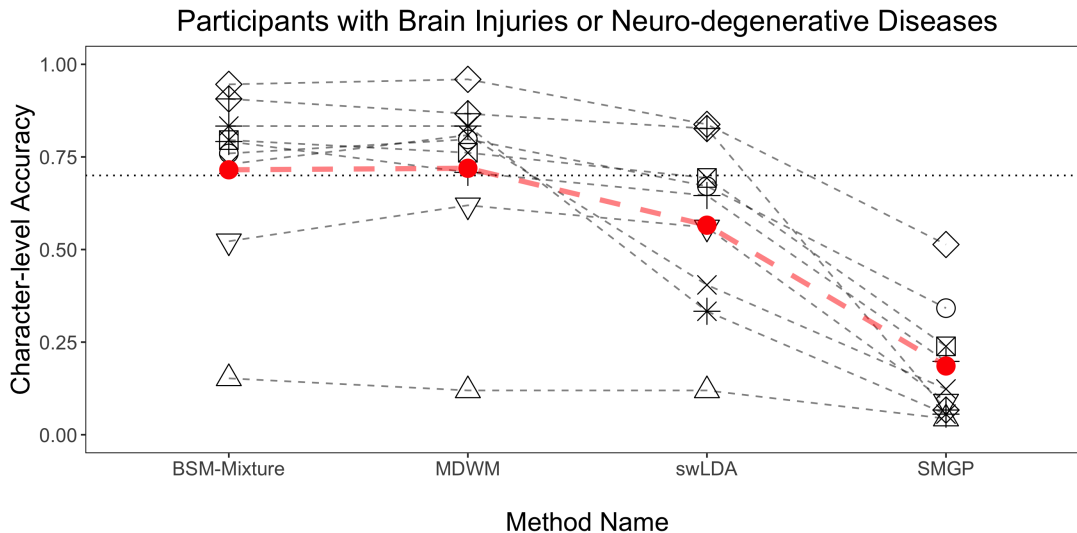


Figure 6: A Spaghetti plot of character-level testing accuracy by BSM-Mixture, MDWM,, swLDA, and SMGP for 9 participants with five training sequences. Means of each method are shown in red. A minimum accuracy of 0.7 for practical usage is shown.

accuracy for communication is considered to be 70% (Kübler and Neumann, 2005). The improvement in BSM-Mixture shows that people with brain injuries or neuro-degenerative diseases benefit from data borrowing.

There are some limitations to our study. First, the generative base classifier we used is still sensitive to background noise compared to other discriminant classifiers. It might overly extract information from source participants to overfit the model. Second, the generative classifier might require tuning hyper-parameters such as the kernel hyper-parameter selection of Gaussian process priors although our sensitivity analysis suggests that the inference and prediction are robust with respect to moderate changes of kernel hyper-parameters. The current strategy is to determine the values with heuristics, which might potentially affect the inference results and the prediction accuracy. Finally, although selection at the participant level is an intuitive idea, the characteristic of heterogeneity over time within the same participant suggested that we should have secondary sequence-level binary selection indicators. However, a side analysis of using sequence-level BSM-Mixture surprisingly

performs worse than the one using participant-level selection indicators. It might be due to the fact that such refined selection indicators paired with generative base classifiers might overfit the training data and therefore has less power to generalize to the FRT data over time. Nevertheless, our main contribution is to demonstrate the advantages of the proposed hierarchical signal-matching framework, and the current framework could definitely be expanded and improved.

For future work, first, we would replace the generative base classifier with other robust discriminant classifiers, e.g., Riemannian geometry. The entire framework would remain unchanged except that we would specify the likelihood function by introducing Riemannian Gaussian distributions (Zanini et al., 2016), (Said et al., 2017). If we followed the generative pathway for classifiers, it could be further improved by adopting the split-and-merge concept to explicitly control the discrepancies between target and non-target (transformed) EEG signals. Finally, we would incorporate our framework into calibration-free methods (Verhoeven et al., 2017). In addition to borrowing the training data from source participants and testing separately, we would directly start testing on the new participant and dynamically update the parameters of the baseline group as the data arrive.

Data Available Statement Since the participants in the original study did not consent to release their data in public directly, even for de-identified version. However, the de-identified data are available upon request for other researchers. An outgoing data user agreement (DUA) will be required to initiate the data transfer. Please contact the corresponding author for details.

7 Acknowledgments

The authors would like to thank the Editor Professor Michael Stein, the Associate Editor and reviewers for their helpful comments and constructive suggestions, which led to this

much-improved manuscript. The authors would also like to acknowledge the participants in our BCI experiments. The content is solely the responsibility of the authors and does not represent the official viewpoints of NICHD, NIH, NIDRR, or the Department of Education.

8 Disclosures

This work was partially supported by grants NIH R01DA048993 (Kang and Johnson), NIH R01MH105561 (Guo and Kang), and NSF IIS2123777 (Kang). The authors have no conflicts of interests to declare.

References

- Adair, J., Brownlee, A., Daolio, F., and Ochoa, G. (2017). Evolving training sets for improved transfer learning in brain computer interfaces. In *International Workshop on Machine Learning, Optimization, and Big Data*, pages 186–197. Springer.
- An, X., Zhou, X., Zhong, W., Liu, S., Li, X., and Ming, D. (2020). Weighted subject-semi-independent erp-based brain-computer interface. In *2020 42nd Annual International Conference of the IEEE Engineering in Medicine & Biology Society (EMBC)*, pages 2969–2972. IEEE.
- Barachant, A., Bonnet, S., Congedo, M., and Jutten, C. (2011). Multiclass brain–computer interface classification by riemannian geometry. *IEEE Transactions on Biomedical Engineering*, 59(4):920–928.
- Barachant, A. and Congedo, M. (2014). A plug&play p300 bci using information geometry. *arXiv preprint arXiv:1409.0107*.
- Bozinovski, S. and Fulgosi, A. (1976). The influence of pattern similarity and transfer

- learning upon training of a base perceptron b2. In *Proceedings of Symposium Informatica*, pages 3–121.
- Cecotti, H. and Graser, A. (2010). Convolutional neural networks for p300 detection with application to brain-computer interfaces. *IEEE transactions on pattern analysis and machine intelligence*, 33(3):433–445.
- Congedo, M., Barachant, A., and Andreev, A. (2013). A new generation of brain-computer interface based on riemannian geometry. *arXiv preprint arXiv:1310.8115*.
- Dawid, A. P. (1981). Some Matrix-variate Distribution Theory: Notational Considerations and a Bayesian Application. *Biometrika*, 68(1):265–274.
- Dixon, M. and Crepey, S. (2018). Multivariate gaussian process regression for portfolio risk modeling: Application to cva. *Department of Applied Mathematics, Illinois Institute of Technology, 2018*.
- Donchin, E., Spencer, K. M., and Wijesinghe, R. (2000). The Mental Prosthesis: Assessing the Speed of a P300-based Brain-computer Interface. *IEEE Transactions on Rehabilitation Engineering*, 8(2):174–179.
- Farwell, L. A. and Donchin, E. (1988). Talking off the top of your head: toward a mental prosthesis utilizing event-related brain potentials. *Electroencephalography and clinical Neurophysiology*, 70(6):510–523.
- Gelman, A. and Rubin, D. B. (1992). Inference from Iterative Simulation using Multiple Sequences. *Statistical Science*, 7(4):457–472.
- Guy, M. W., Conte, S., Bursahoglu, A., and Richards, J. E. (2021). Peak selection and latency jitter correction in developmental event-related potentials. *Developmental psychobiology*, 63(7):e22193.

- Kaper, M., Meinicke, P., Grossekhoefer, U., Lingner, T., and Ritter, H. (2004). BCI Competition 2003-data Set IIB: Support Vector Machines for the P300 Speller Paradigm. *IEEE Transactions on Biomedical Engineering*, 51(6):1073–1076.
- Khazem, S., Chevallier, S., Barthélemy, Q., Haroun, K., and Noûs, C. (2021). Minimizing subject-dependent calibration for bci with riemannian transfer learning. In *2021 10th International IEEE/EMBS Conference on Neural Engineering (NER)*, pages 523–526. IEEE.
- Krusienski, D. J., Sellers, E. W., McFarland, D. J., Vaughan, T. M., and Wolpaw, J. R. (2008). Toward Enhanced P300 Speller Performance. *Journal of Neuroscience Methods*, 167(1):15–21.
- Kübler, A. and Neumann, N. (2005). Brain-computer interfaces—the key for the conscious brain locked into a paralyzed body. *Progress in brain research*, 150:513–525.
- Lenzerini, M. (2002). Data integration: A theoretical perspective. In *Proceedings of the twenty-first ACM SIGMOD-SIGACT-SIGART symposium on Principles of database systems*, pages 233–246.
- Li, F., Xia, Y., Wang, F., Zhang, D., Li, X., and He, F. (2020). Transfer learning algorithm of p300-eeeg signal based on xdawn spatial filter and riemannian geometry classifier. *Applied Sciences*, 10(5):1804.
- Ma, T., Li, Y., Huggins, J. E., Zhu, J., and Kang, J. (2022). Bayesian inferences on neural activity in eeg-based brain-computer interface. *Journal of the American Statistical Association*, 117(539):1122–1133.
- Niedermeyer, E. and da Silva, F. L. (2005). *Electroencephalography: basic principles, clinical applications, and related fields*. Lippincott Williams & Wilkins.

- Rivet, B., Souloumiac, A., Attina, V., and Gibert, G. (2009). x dawn algorithm to enhance evoked potentials: application to brain–computer interface. *IEEE Transactions on Biomedical Engineering*, 56(8):2035–2043.
- Rodrigues, P. L. C., Jutten, C., and Congedo, M. (2018). Riemannian procrustes analysis: transfer learning for brain–computer interfaces. *IEEE Transactions on Biomedical Engineering*, 66(8):2390–2401.
- Said, S., Bombrun, L., Berthoumieu, Y., and Manton, J. H. (2017). Riemannian gaussian distributions on the space of symmetric positive definite matrices. *IEEE Transactions on Information Theory*, 63(4):2153–2170.
- Thompson, D. E., Gruis, K. L., and Huggins, J. E. (2014). A Plug-and-play Brain-computer Interface to Operate Commercial Assistive Technology. *Disability and Rehabilitation: Assistive Technology*, 9(2):144–150.
- Verhoeven, T., Hübner, D., Tangermann, M., Müller, K.-R., Dambre, J., and Kindermans, P.-J. (2017). Improving zero-training brain-computer interfaces by mixing model estimators. *Journal of neural engineering*, 14(3):036021.
- Wu, D., Xu, Y., and Lu, B.-L. (2020). Transfer learning for eeg-based brain–computer interfaces: A review of progress made since 2016. *IEEE Transactions on Cognitive and Developmental Systems*, 14(1):4–19.
- Xu, M., Liu, J., Chen, L., Qi, H., He, F., Zhou, P., Cheng, X., Wan, B., and Ming, D. (2015). Inter-subject information contributes to the erp classification in the p300 speller. In *2015 7th International IEEE/EMBS Conference on Neural Engineering (NER)*, pages 206–209. IEEE.
- Xu, M., Liu, J., Chen, L., Qi, H., He, F., Zhou, P., Wan, B., and Ming, D. (2016).

Incorporation of inter-subject information to improve the accuracy of subject-specific p300 classifiers. *International journal of neural systems*, 26(03):1650010.

Xu, N., Gao, X., Hong, B., Miao, X., Gao, S., and Yang, F. (2004). Bci competition 2003-data set iib: enhancing p300 wave detection using ica-based subspace projections for bci applications. *IEEE transactions on biomedical engineering*, 51(6):1067–1072.

Zanini, P., Congedo, M., Jutten, C., Said, S., and Berthoumieu, Y. (2016). Parameters estimate of riemannian gaussian distribution in the manifold of covariance matrices. In *2016 IEEE Sensor Array and Multichannel Signal Processing Workshop (SAM)*, pages 1–5. IEEE.

Zhang, L., Banerjee, S., and Finley, A. O. (2021). High-dimensional multivariate geostatistics: A bayesian matrix-normal approach. *Environmetrics*, 32(4):e2675.